

Surface band bending and interface alignment of plasma-enhanced atomic layer deposited SiO₂ on Al_xGa_{1-x}N

Cite as: J. Appl. Phys. **122**, 125304 (2017); <https://doi.org/10.1063/1.5003921>

Submitted: 16 May 2017 • Accepted: 07 September 2017 • Published Online: 29 September 2017

Brianna S. Eller and Robert J. Nemanich



View Online



Export Citation



CrossMark

ARTICLES YOU MAY BE INTERESTED IN

Surface band bending and band alignment of plasma enhanced atomic layer deposited dielectrics on Ga- and N-face gallium nitride

Journal of Applied Physics **116**, 123702 (2014); <https://doi.org/10.1063/1.4895985>

Impact of N₂ and forming gas plasma exposure on the growth and interfacial characteristics of Al₂O₃ on AlGaN

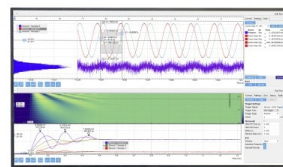
Applied Physics Letters **103**, 221604 (2013); <https://doi.org/10.1063/1.4833836>

Cleaning of AlN and GaN surfaces

Journal of Applied Physics **84**, 5248 (1998); <https://doi.org/10.1063/1.368814>

Challenge us.

What are your needs for periodic signal detection?



Zurich
Instruments



Surface band bending and interface alignment of plasma-enhanced atomic layer deposited SiO₂ on Al_xGa_{1-x}N

Brianna S. Eller and Robert J. Nemanich

Department of Physics, Arizona State University, Tempe, AZ 85287-1504, USA

(Received 16 May 2017; accepted 7 September 2017; published online 29 September 2017)

Al_xGa_{1-x}N is characterized by a significant spontaneous and piezoelectric polarization, which increases with the aluminum content. As a result, a surface bound charge is present, which favors compensation by surface states and influences the reliability of AlGaN/GaN devices. This work, therefore, focused on the effects of the polarization charge for GaN and AlGaN with three different aluminum concentrations 15%, 25%, and 35%. The band bending of Al_xGa_{1-x}N surfaces was measured after a N₂/H₂ plasma pretreatment, which reduced the carbon and oxygen contamination below the detection limit of x-ray photoelectron spectroscopy. Surface band bending was then related to surface states, where the band bending of oxygen-free surfaces—as obtained with a high-temperature, immersed hydrogen/nitrogen plasma clean—scales with the aluminum content. In addition, the band offsets at the plasma-enhanced atomic layer deposited SiO₂/Al_xGa_{1-x}N interface were measured, giving 3.4 eV, 3.3 eV, 3.3 eV, and 3.0 eV for respective 0%, 15%, 25%, and 35% aluminum concentrations. These values are in accordance with the charge neutrality level model, which implies that SiO₂ will confine carriers over nearly the full range of the aluminum content.

Published by AIP Publishing. [<http://dx.doi.org/10.1063/1.5003921>]

I. INTRODUCTION

AlGaN/GaN heterostructures have demonstrated considerable promise for power and RF applications due to material properties such as the wide bandgap, high bulk thermal conductivity, and high breakdown field. Moreover, AlGaN and GaN are characterized by a spontaneous and piezoelectric polarization, where the polarization of Al_xGa_{1-x}N increases with aluminum content x . Consequently, Ga-face AlGaN/GaN heterostructures exhibit an overall positive polarization charge at the interface, which engenders a two-dimensional electron gas (2DEG). This phenomenon enables low-resistance operation of high-electron mobility transistors (HEMTs). However, AlGaN/GaN HEMTs and HFETs are also characterized by relatively large leakage current and current collapse. The states responsible for these reliability issues may be related to compensation charge, where the large polarization of these materials produces significant surface bound charge that favors external compensation.¹ This work, therefore, investigates the effects of polarization and aluminum content at the GaN and AlGaN surfaces and at the dielectric interfaces.

Dielectrics have been used to mitigate reliability issues. An ideal gate dielectric is characterized by a large bandgap, which results in a conduction band offset large enough to provide an effective barrier for gate leakage, as well as a high dielectric constant, which enables high voltage operation and lowers equivalent oxide thicknesses.² Unfortunately, these characteristics are inversely related; Fig. 1 shows the inverse of the bandgap dependent on the electronic component of the dielectric constant, which is characterized by a linear trend as determined by the Moss relation.^{3,4} Of these common dielectrics, SiO₂ is characterized by the largest bandgap and thus most likely to confine carriers. Recent works⁵⁻⁷ have investigated SiO₂ due to its potential to reduce gate leakage. The trade-off is

a low dielectric constant, which reduces the effective oxide thickness and limits device scalability. Therefore, SiO₂ utilized in state-of-the-art vertical GaN technologies⁸⁻¹¹ is often incorporated with higher- k dielectrics—e.g., high- k HfAlO capped with a SiO₂ passivation layer—in an attempt to achieve a dielectric passivation structure with both a high bandgap and a high- k dielectric constant.^{7,8,12-14}

In this work, we investigated the electronic state configuration of oxygen-free Al_xGa_{1-x}N surfaces—as obtained with a high-temperature, immersed hydrogen/nitrogen plasma clean—and plasma-enhanced atomic layer deposited (PEALD) SiO₂/Al_xGa_{1-x}N interfaces, where PEALD provides higher-quality films in comparison to many other deposition techniques in terms of stoichiometry, breakdown field, and high defect density.^{15,16} Moreover, this technique deposits uniform and conformal films with precise thickness control.¹⁷ Thin (~ 3 nm) SiO₂ layers were deposited and characterized by x-ray photoelectron spectroscopy (XPS) to determine the interface electronic state configuration. Characterization was also performed on Al_xGa_{1-x}N surfaces, thus determining the polarization and aluminum concentration effects on both surface and interface states.

II. EXPERIMENT

Ga-face, n-type Al_xGa_{1-x}N samples were purchased from NTT Advanced Technology. Samples were ~ 50 nm thick as deposited on silicon substrates intentionally doped with silicon at a doping density of $\sim 10^{17}$ cm⁻³, which is used to determine the position of the Fermi level in this research. In addition, four different concentrations of aluminum—0%, 15%, 25%, and 35%—provided varied bandgaps and surface polarization conditions, as summarized in Table I. An uncertainty of 0.1 eV is assumed for the bandgap values.

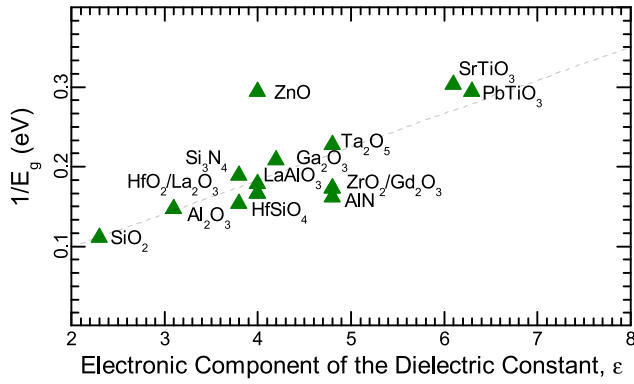


FIG. 1. Inverse of the bandgap with respect to the electronic component of the dielectric constant for various dielectrics. This trend is characterized by the Moss relation:³ $1/E_g = K \epsilon_\infty + C$, where both K and C are constants equivalent to 0.043 eV^{-1} and 0.013 eV^{-1} , respectively, for the given relation.

TABLE I. Characteristics of $\text{Al}_x\text{Ga}_{1-x}\text{N}$ as determined by the linear interpolation of GaN and AlN properties.

Al-content, x	E_g (eV)	Fermi level (eV below CB)
0%	3.40	0.06
15%	3.82	0.07
25%	4.10	0.08
35%	4.38	0.08

$\text{Al}_x\text{Ga}_{1-x}\text{N}$ samples were cleaned *ex-situ* via sonication in acetone, methanol, and ammonia hydroxide for 10 min each followed by rinsing with deionized water and N_2 blow drying. Samples were then transferred to an ultra-high vacuum system for *in-situ* cleaning, ALD, and processing. Plasma cleaning was conducted at 680°C in an immersed (4:1) N_2/H_2 rf plasma ignited at 300 W. This cleaning maintained the substrate stoichiometry and reduced both the carbon contamination and oxygen coverage on the surface below the detection limit of XPS, thereby determining an “oxygen-free” surface as shown in Fig. 2.

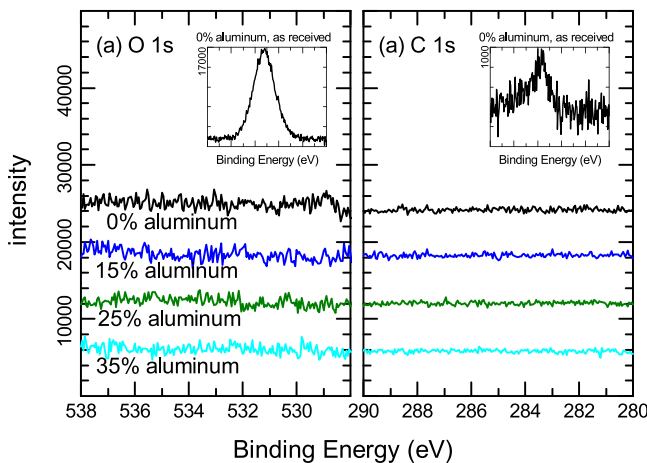


FIG. 2. XPS spectra of residual oxygen (left) and carbon (right) contamination before (inset) and after 680°C N_2/H_2 plasma surface treatment. For both elements, the contamination levels were below the detection limit of the XPS.

Oxygen-free surfaces were used to determine the difference between the valence band maximum (E_{VBM}) and binding energy of the Ga 3d core level (E_{Ga3d}), $E_{Ga3d} - E_{VBM}$, and the band bending of clean $\text{Al}_x\text{Ga}_{1-x}\text{N}$. These characteristics were determined by monochromated XPS. E_{VBM} was linearly extrapolated from the low binding energy cutoff within a tenth of an eV, and E_{Ga3d} was determined by peak fitting within half a tenth of an eV.

After cleaning, remote plasma-enhanced atomic layer deposition (PEALD) was used to deposit $\sim 3 \text{ nm}$ SiO_2 . During deposition, oxygen plasma was ignited at 200 W at a pressure of $\sim 100 \text{ mTorr}$ and a flow rate of 35 sccm. The PEALD process using tri(dimethylamino)silane (TDMAS)¹⁸ was adopted for this work, including 1.6 s TDMAS, 16 s O_2 plasma, and 40 s N_2 purge at room temperature. Following deposition, samples were annealed at 400°C in 60 mTorr N_2 ambient for 30 min to reduce the higher oxygen content typical of PEALD films. The result is stoichiometric SiO_2 with a density of $2.2 \pm 0.2 \text{ g/cm}^3$ as determined by Rutherford backscattering spectrometry and x-ray reflectivity.

III. RESULTS AND DISCUSSION

A. Valence band maximum and surface states on $\text{Al}_x\text{Ga}_{1-x}\text{N}$

Measured values for $(E_{Ga3d} - E_{VBM})_{\text{Al}_x\text{Ga}_{1-x}\text{N}}$ for oxygen-free surfaces are summarized in Fig. 3, and the corresponding values for E_{Ga3d} and E_{VBM} are given in Table II. According to other electronic-state studies, $(E_{Ga3d} - E_{VBM})_{\text{GaN}}$ is in the range of 17.7–17.8 eV,^{19–21} thus, this value has been used in our previous studies.^{22,23,26} Similar electronic-state studies of $\text{Al}_{0.25}\text{Ga}_{0.75}\text{N}$ indicated that 17.5 eV²⁴ is the respective difference. The measured values are summarized in Table III.

Since E_{VBM} is intricately related to surface states, the discrepancy in these values could be related to the surface termination of the samples, which can vary considerably for

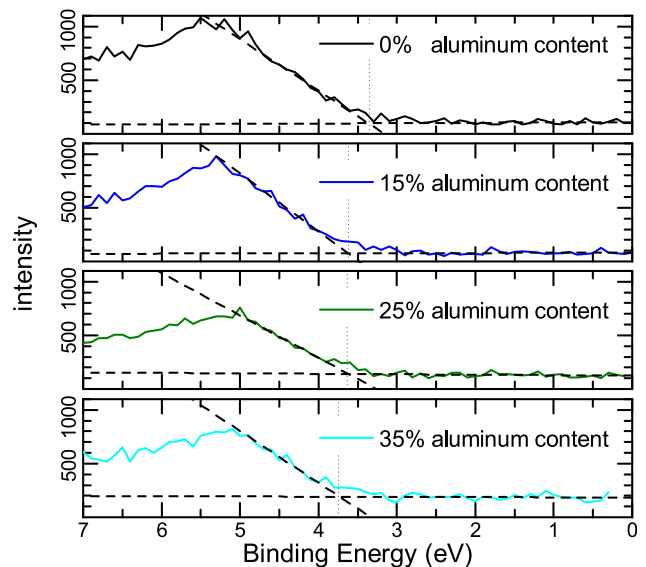


FIG. 3. VBM of $\text{Al}_x\text{Ga}_{1-x}\text{N}$ as determined by XPS. (NOTE: the Ga 3d peaks were aligned to allow for more direct comparison of the VBMs.)

TABLE II. Position of VBM with an uncertainty of ± 0.10 and the Ga 3d core level with an uncertainty of ± 0.05 of $\text{Al}_x\text{Ga}_{1-x}\text{N}$.

Al-content, x	$E_{\text{Ga}3d}$ (eV)	E_{VBM} (eV)
0%	20.59	3.17
15%	20.91	3.72
25%	20.48	3.41
35%	20.40	3.33

TABLE III. Values of $(E_{\text{Ga}3d} - E_{\text{VBM}})_{\text{Al}_x\text{Ga}_{1-x}\text{N}}$, expected and measured with an uncertainty of ± 0.17 . Some of these values were determined by linear interpolation as noted by “interp.” The measured value was ~ 0.4 eV below the expected values.

Al-content, x	$E_{\text{Ga}3d} - E_{\text{VBM}}$ (eV)		
	Measured	Expected	References
0%	17.42	17.76	19–21
15%	17.19	17.63	Interp.
25%	17.07	17.54	24
35%	17.07	17.45	Interp.

GaN and AlGaN surfaces. In the work presented by Waldrop and Grant,²⁰ GaN and AlN were grown *in-situ* by molecular beam epitaxy. The resulting surface was characterized by a hexagonal 1×1 low energy electron diffraction pattern, indicating the epitaxial surface. This work determined $(E_{\text{Ga}3d} - E_{\text{VBM}})_{\text{GaN}}$ for these surfaces as 17.8 eV. In the study by Cook *et al.*,^{19,25} GaN surfaces were cleaned at 860 °C for 15 min in a NH_3 atmosphere. The NH_3 gas anneal effectively produced an oxygen-free surface, and the results suggested that $(E_{\text{Ga}3d} - E_{\text{VBM}})_{\text{GaN}}$ was 17.7 eV. In this work, surfaces were also oxygen free but processed with a different surface treatment.

To investigate the relationship between surface states and preparation treatment, an alternative plasma clean was also conducted on a GaN surface. This clean included a 680 °C NH_3 plasma anneal followed by a N_2 gas anneal for 15 min each, as used in a previous study.²⁶ This plasma surface treatment results in ~ 1 ML of oxygen coverage on the surface. This clean resulted in an oxygen-terminated GaN surface, where the oxygen-terminated surface was characterized by an

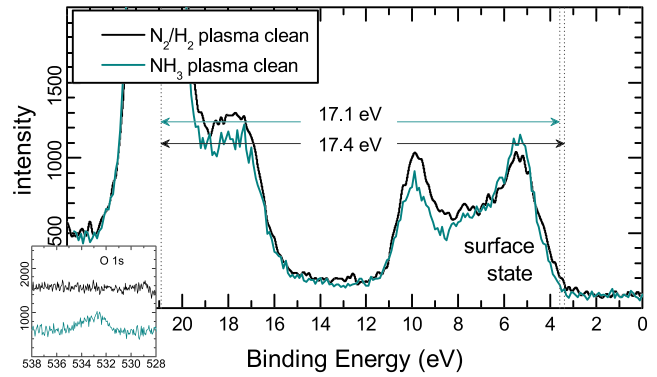


FIG. 4. XPS of the Ga 3d core level to VBM of GaN after different plasma treatments, resulting in different surface states. One clean results in an oxygen-free surface, while the other gives ~ 1 ML of oxygen coverage as shown by the O 1s core level in the inset. (NOTE: Ga 3d peaks were aligned to account for differences in band bending.)

$E_{\text{Ga}3d}$ of 21.1 eV and an E_{VBM} of 4.0 eV as shown in Fig. 4. Thus, $(E_{\text{Ga}3d} - E_{\text{VBM}})_{\text{GaN}}$ was 17.1 eV. In addition, the valence band edge of the oxygen-free surface is characterized by a surface state feature above the bulk VBM that is not observed on the oxygen-terminated surface. Moreover, in addition to the difference in oxygen coverage, the NH_3 cleaning processes also resulted in less NH_x as shown in Fig. 5. (NOTE: Surface-sensitive Ga Auger and Ga 2p peaks also suggest that NH_3 plasma and N_2/H_2 plasma treatments produce different surface terminations likely related to the differences in oxygen coverage.)

This value for $E_{\text{Ga}3d} - E_{\text{VBM}}$ of oxygen-terminated GaN agrees with another study presented by Martin *et al.*²⁷ In this work, samples were grown *in-situ*; however, E_{VBM} was determined by aligning prominent features in the valence band rather than from the valence band edge. Consequently, although the surface would be characterized by a similar surface state as in previously mentioned studies, the method of calculation likely overlooked this state. In other words, this measurement demonstrated the influence of a surface state. The surface state above the bulk VBM potentially obscures the valence band edge and thus appears to shift the valence band towards lower binding energy. This “shift” would consequently increase $(E_{\text{Ga}3d} - E_{\text{VBM}})_{\text{GaN}}$ and thus account for the difference in $E_{\text{Ga}3d} - E_{\text{VBM}}$ values. This explanation is consistent

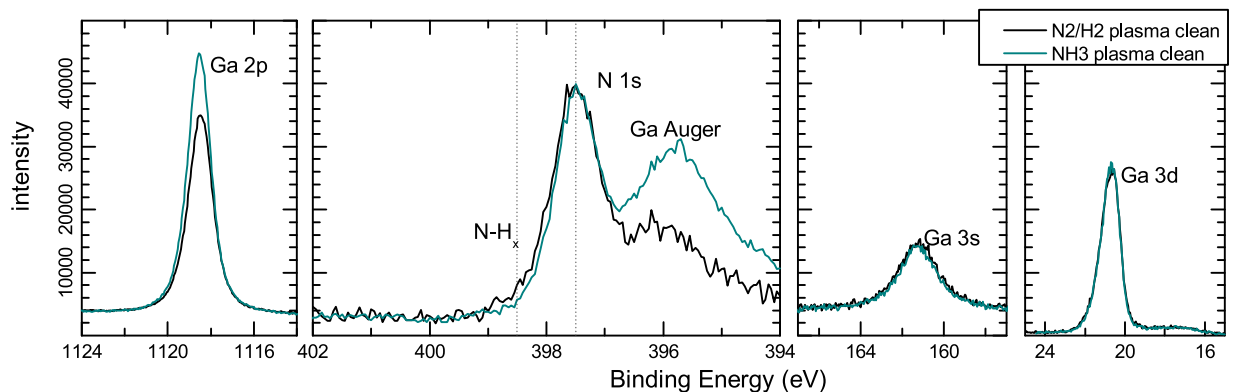


FIG. 5. XPS of Ga 3d, Ga 3s, N 1s, and Ga 2p core levels of GaN dependent on plasma surface cleaning. (Note: the core levels of the NH_3 cleaned samples were shifted to lower binding energy by ~ 0.6 eV to account for the difference in band bending and enable better comparison between bonding states.)

with other surface studies of GaN, which agree that there is at least one surface state at or just above the bulk VBM that is sensitive to adsorption—according to a detailed review by Bermudez.²⁸

For the following calculations, expected values were used, where discrepancies in $E_{Ga3d}-E_{VBM}$ may result in some additional error of approximately ± 0.2 eV.

B. Surface band bending and states on $Al_xGa_{1-x}N$

Band bending at the surface was also determined by E_{Ga3d} . Previous work by Eller *et al.*¹ measured the band bending of N-face GaN, Ga-face GaN, and Ga-face $Al_{0.25}Ga_{0.75}N$ surfaces after various cleaning steps as related to the net surface charge. The results showed that band bending was virtually independent of polarization, where all three surfaces exhibited the same upward band bending. Surface states, therefore, compensated any differences in the magnitude and/or direction of the bound surface polarization charge, where the position of the Fermi level with respect to the conduction band was pinned ~ 0.4 eV below the conduction band minimum. However, in this work, the results demonstrate different behaviors, where band bending increases with the aluminum content or polarization bound charge as shown in Table IV. Band bending is related to the net surface compensation charge

$$N_{CC} = N_{SS} - N_{PBC} = \sqrt{\frac{2\Phi_s \epsilon \epsilon_0 N_d}{q}} - N_{PBC}, \quad (1)$$

where N_{SS} is the total net surface states in charges/cm² including the polarization bound charge or N_{PBC} , Φ_s is the measured band bending, ϵ is the relative permittivity, ϵ_0 is the permittivity of free space, N_d is the doping density, and q is the charge of an electron.

It is also worth noting that surface photovoltage effects influence spectroscopy-based band bending measurements and thus reduced observed band bending. In other words, band bending at the surface is slightly larger than XPS measurements would suggest by ~ 0.3 eV.²⁹ Consequently, the net surface compensation charge may be slightly underestimated by $\sim 5.6 \times 10^{11}$ charges/cm² in this study.

For oxygen-free surfaces, the compensation charge scales with the aluminum content and thus the magnitude of the polarization bound charge. This behavior varies from previous work, which observed similar band bending regardless of the magnitude or direction of polarization charge.^{1,30}

The key difference is that previous reports presented results for oxygen-terminated surfaces, whereas the results presented here are for oxygen-free surfaces. The difference in surface behavior is, thus, likely related to oxygen states. A study by Higashiwaki *et al.*^{31,32} showed that oxidized AlGaN surfaces reconstruct such that oxygen-related states behave like donors, whereas Miao *et al.*³³ suggested that these donor states are likely related to substitutional oxygen (O_N). These states may, therefore, explain the pinning behavior noted on the oxygen-terminated surfaces but not the oxygen-free.³⁴ However, it is also worth noting that other electrochemical studies have also demonstrated similar upwards band bending, which is explained as the result of states near or at the surface—within 1 eV of the CB—and of a similar density.^{12,30,34} In other words, both the “oxygen-terminated” and “oxygen-free” surfaces are characterized by the significant surface compensation charge on the order of $+10^{13}$ charges/cm²; it is thus likely that the nitrogen vacancies and/or gallium dangling bonds also interact as surface states.

C. Interface band offsets of PEALD $SiO_2/Al_xGa_{1-x}N$

After the deposition of PEALD SiO_2 , the measured XPS spectra—as summarized in Table V—were used to determine the energy difference between respective core levels; this difference subsequently reveals the valence band offsets (VBOs)

$$\Delta E_V = (E_{Ga3d} - E_{VBM})_{Al_xGa_{1-x}N} - (E_{Si2s} - E_{VBM})_{SiO_2} + \Delta E_{CL}, \quad (2)$$

where $(E_{Si2s}-E_{VBM})_{SiO_2}$ was determined to be 149.0 eV—similar to the previously reported value of 148.9 eV.²⁶ ΔE_{CL} is the difference between the respective Si 2s and Ga 3d core levels, i.e., $E_{Si2s} - E_{Ga3d}$. The relationship between VBOs and the aluminum content is summarized in Table VI, which is in agreement with previous results.²⁶ Conduction band offsets are determined using the bandgaps of $Al_xGa_{1-x}N$ as summarized in Table I and bandgaps of SiO_2 as 8.9 eV.

Note that the band offsets shift after annealing. Since band offsets are typically constant between two materials as determined by interfacial bonding, this shift is likely related to a potential drop across the interfacial layer.^{18,22} Although surfaces are oxygen free prior to deposition, it is likely that a thin subcutaneous oxide layer forms during PEALD, ~ 1 nm thick. Acceptor-like defects are also introduced during the

TABLE IV. Surface charge distribution of $Al_xGa_{1-x}N$, where compensation charge is determined from measured band bending and calculated bound polarization charge, which is presented with an uncertainty of ± 0.15 . (Please note that surface photovoltage effects are not accounted for in these measurements, which could potentially result in a ~ 0.3 eV reduction in the band bending and a subsequent $\sim 0.056 \times 10^{13}$ charges/cm² increase in net surface compensation charge.)

Al-content, x	Spontaneous polarization (C/m ²)	Polarization bound charge ($\times 10^{13}$ charges/cm ²)	Band bending (eV)	Net surface compensation charge ($\times 10^{13}$ charges/cm ²)
0%	-0.029	-1.81	0.51 eV	+1.74
15%	-0.037	-2.30	0.47 eV	+2.23
25%	-0.042	-2.62	1.08 eV	+2.51
35%	-0.047	-2.95	1.35 eV	+2.83

TABLE V. Core level results for Ga 3d, Al 2p, Ga 3s, Si 2s, and O 1s spectra of ~ 3 nm PEALD-deposited SiO_2 on $\text{Al}_x\text{Ga}_{1-x}\text{N}$, including the peak position center and full-width half-maximum (FWHM). All energies are rounded to the nearest tenth and given in eV.

Al-content, x	$\text{SiO}_2/\text{Al}_x\text{Ga}_{1-x}\text{N}$ as deposited										$\text{SiO}_2/\text{Al}_x\text{Ga}_{1-x}\text{N}$ annealed									
	Ga 3d		Al 2p		Ga 3s		Si 2s		O 1s		Ga 3d		Al 2p		Ga 3s		Si 2s		O 1s	
	center	FWHM	center	FWHM	center	FWHM	center	FWHM	center	FWHM	center	FWHM	center	FWHM	center	FWHM	center	FWHM	center	FWHM
0%	20.5	1.1	—	—	161.1	2.5	155.3	2.4	533.8	1.4	20.5	1.1	—	—	161.0	2.2	155.2	2.3	533.6	1.4
15%	20.8	1.1	75.3	1.5	161.5	2.0	155.6	2.0	534.4	1.4	20.9	1.1	75.3	1.6	161.5	2.0	155.6	2.1	534.0	1.4
25%	20.5	1.1	74.5	1.4	161.0	2.5	155.3	2.2	533.8	1.5	20.4	1.1	74.5	1.4	161.1	2.4	155.2	2.3	533.5	1.4
35%	20.2	1.2	74.2	1.4	160.7	3.1	155.1	2.5	533.6	1.5	20.4	1.2	74.4	1.3	160.9	2.7	154.9	2.3	533.2	1.4

TABLE VI. VBOs as determined from XPS Si 2s and Ga 3d core levels with an experimental uncertainty of ± 0.17 . The conduction band offset is determined from the known bandgaps of the materials, where the bandgap of SiO_2 is 8.9 eV.

Al-content, x	$\text{SiO}_2/\text{Al}_x\text{Ga}_{1-x}\text{N}$ as deposited (eV)		$\text{SiO}_2/\text{Al}_x\text{Ga}_{1-x}\text{N}$ annealed (eV)	
	VBO	CBO	VBO	CBO
0%	3.47	2.03	3.37	2.13
15%	3.32	1.76	3.32	1.76
25%	3.36	1.44	3.26	1.54
35%	3.15	1.37	2.95	1.57

growth process, generating an electric field in this interfacial layer. Subsequent annealing removes this charge and reduces the electric field across the interfacial layer.

The results demonstrate the difference in the bandgap as a result of the aluminum content largely manifesting in the conduction band rather than in the valence band. Figure 6 compares measured band offsets after annealing with those calculated by the charge neutrality level (CNL) model, which argues that the interface of two materials will align at the charge neutrality level. The CNL of SiO_2 is reported at 4.5 eV, while those of GaN and AlN are reported at 2.3 and 2.8 eV above the respective valence band.³⁵ The CNL of $\text{Al}_x\text{Ga}_{1-x}\text{N}$ is thus determined from linear interpolation: $\text{CNL}_{\text{AlGa}}(x) = 2.8x + 2.3(1-x)$. It is evident from this model that the difference in bandgap is largely manifested in the conduction band.

In terms of increased polarization, this behavior is unexpected. As noted by Mönch,³⁶ increased polarity generally results in two effects: (1) the valence band flattens as it corresponds to the higher effective hole mass and (2) the conduction bands become less direct with respect to the valence band maximum. This redistribution of the density of states pushes the charge neutrality level higher in the bandgap. Consequently, the difference in the bandgap manifests most significantly in the valence band. However, for GaN and

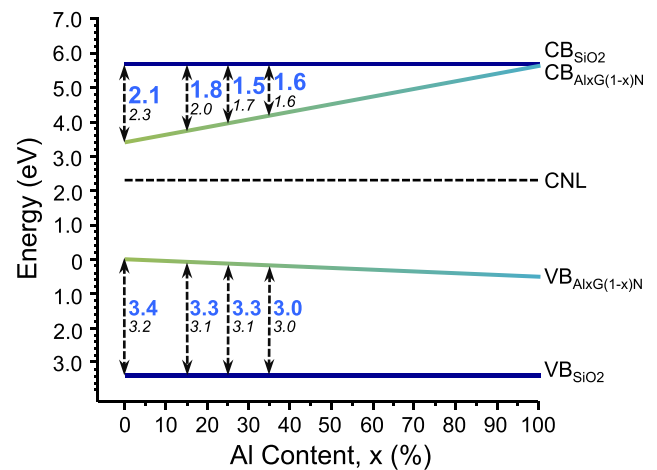


FIG. 6. Band alignment as determined by the charge neutrality level model. Experimental offset measurements are rounded to the nearest tenth and given in blue followed by the theoretical results for comparison. The theory is linearly interpolated from the CNLs given by Robertson and Falabretti.³⁵

AlN, both materials are direct semiconductors. In addition, the effective hole masses suggest slightly flatter bands for AlN. Similarly, the electron effective mass suggests that the conduction band is slightly flatter for AlN. However, this effect is more significant for the conduction band than the valence band. Thus, the higher density of states in the conduction band compensates the flattening valence band.³⁷ Therefore, the CNL does not move as far up in the bandgap as polarization would suggest, and the difference in bandgap is largely manifested in the conduction band.³⁸

IV. CONCLUSIONS

In summary, this work discussed band bending and alignment characteristics of oxygen-free $\text{Al}_x\text{Ga}_{1-x}\text{N}$ surfaces and PEALD $\text{SiO}_2/\text{Al}_x\text{Ga}_{1-x}\text{N}$ interfaces for 0%, 15%, 25%, and 35% aluminum contents. A 680 °C N_2/H_2 plasma surface pretreatment reduced oxygen and carbon coverage below XPS detection, producing an “oxygen-free” surface. The variation in band bending dependent on the aluminum content—and thus the magnitude of surface polarization bound charge—was observed, where previous studies of oxygen-terminated surfaces observed similar band bending regardless of the magnitude or direction of surface polarization bound charge. These results suggest that donor-like oxygen states are responsible for the Fermi level pinning characteristic of GaN.

Valence band offsets for PEALD $\text{SiO}_2/\text{Al}_x\text{Ga}_{1-x}\text{N}$ were also determined, giving 3.4 eV, 3.3 eV, 3.3 eV, and 3.0 eV for respective concentrations of aluminum. These values are in accordance with the charge neutrality level model and indicate that SiO_2 will confine carriers across all concentrations of $\text{Al}_x\text{Ga}_{1-x}\text{N}$.

ACKNOWLEDGMENTS

This research was supported by the Office of Naval Research through the DEFINE MURI program, N00014-10-1-0937, and Advanced Research Projects Agency-Energy through the SWITCHES program, DE-AR0000453. We are also thankful to Dr. Barry Wilkens and Dr. Emmanuel Soignard for providing Rutherford backscattering spectrometry and x-ray reflectivity measurements at the Leroy Eyring Center for Solid-State Science, respectively.

¹B. S. Eller, J. Yang, and R. J. Nemanich, *J. Electron. Mater.* **43**, 4560 (2014).

²B. S. Eller, J. Yang, and R. J. Nemanich, *J. Vac. Sci. Technol. A* **31**, 050807 (2013).

³T. S. Moss, *Phys. Status Solidi B* **131**, 415 (1985).

⁴R. R. Reddy and Y. N. Ahammed, *Infrared Phys. Technol.* **36**, 825 (1995).

⁵B. Lee, C. Kirkpatrick, Y.-H. Choi, X. Yang, A. Q. Huang, and V. Misra, *Phys. Status Solidi* **9**, 868 (2012).

⁶C. J. Kirkpatrick, B. Lee, R. Suri, X. Yang, and V. Misra, *IEEE Electron Device Lett.* **33**, 1240 (2012).

⁷N. Ramanan, B. Lee, C. Kirkpatrick, R. Suri, and V. Misra, *Semicond. Sci. Technol.* **28**, 074004 (2013).

⁸N. Ramanan, B. Lee, and V. Misra, *Semicond. Sci. Technol.* **31**, 035016 (2016).

⁹X. Zou, X. Zhang, X. Lu, C. W. Tang, and K. M. Lau, *IEEE Electron Device Lett.* **37**, 636 (2016).

¹⁰S. K. Oh, T. Jang, Y. J. Jo, H.-Y. Ko, and J. S. Kwak, *Surf. Coat. Technol.* **307**, 1124 (2016).

¹¹C. H. Wang, S. Y. Ho, and J. J. Huang, *IEEE Electron Device Lett.* **37**, 74 (2016).

¹²N. Ramanan, B. Lee, and V. Misra, *IEEE Trans. Electron Devices* **62**, 546 (2015).

¹³F. Roccaforte, P. Fiorenza, G. Greco, R. Lo Nigro, F. Giannazzo, A. Patti, and M. Saggio, *Phys. Status Solidi A* **211**, 2063 (2014).

¹⁴C.-H. Hsu, W.-C. Shih, Y.-C. Lin, H.-T. Hsu, H.-H. Hsu, Y.-X. Huang, T.-W. Lin, C.-H. Wu, W.-H. Wu, J.-S. Maa, H. Iwai, K. Kakushima, and E. Y. Chang, *Jpn. J. Appl. Phys., Part 1* **55**, 04EG04 (2016).

¹⁵L. Han and Z. Chen, *J. Solid-State Sci. Technol.* **2**, N228 (2013).

¹⁶R. L. Puurunen, *J. Appl. Phys.* **97**, 121301 (2005).

¹⁷G. Dingemans, C. A. A. van Helvoirt, M. C. M. van de Sanden, and W. M. M. Kessels, *ECS Trans.* **35**, 191 (2011).

¹⁸B. S. Eller, W. Li, S. Rupperecht, and R. J. Nemanich, “Characterization of plasma-enhanced atomic layer deposition of SiO_2 using tris(dimethylamino)silane on GaN,” (unpublished).

¹⁹T. E. Cook, Jr., C. C. Fulton, W. J. Mccouch, R. F. Davis, G. Lucovsky, and R. J. Nemanich, *J. Appl. Phys.* **94**, 7155 (2003).

²⁰J. R. Waldrop and R. W. Grant, *Appl. Phys. Lett.* **68**, 2879 (1996).

²¹J. Hedman and N. Mårtensson, *Phys. Scr.* **22**, 176 (1980).

²²J. Yang, B. S. Eller, C. Zhu, C. England, and R. J. Nemanich, *J. Appl. Phys.* **112**, 053710 (2012).

²³J. Yang, B. S. Eller, M. Kaur, and R. J. Nemanich, *J. Vac. Sci. Technol. A* **32**, 021514 (2014).

²⁴Y. L. Chiou and C. T. Lee, *IEEE Trans. Electron Devices* **58**, 3869 (2011).

²⁵T. E. Cook, Jr., C. C. Fulton, W. J. Mccouch, K. M. Tracy, R. F. Davis, G. Lucovsky, E. H. Hurt, and R. J. Nemanich, *J. Appl. Phys.* **93**, 3995 (2003).

²⁶J. Yang, B. S. Eller, and R. J. Nemanich, *J. Appl. Phys.* **116**, 123702 (2014).

²⁷G. Martin, S. Strite, A. Botchkarev, A. Agarwal, A. Rockett, H. Morkoc, W. R. L. Lambrecht, and B. Segall, *Appl. Phys. Lett.* **65**, 610 (1994).

²⁸V. M. Bermudez, *Surf. Sci. Rep.* **72**, 147 (2017).

²⁹J. P. Long and V. M. Bermudez, *Phys. Rev. B* **66**, 121308 (2002).

³⁰I. Bartoš, O. Romanyuk, J. Houdkova, P. P. Paskov, T. Paskova, and P. Jiríček, *J. Appl. Phys.* **119**, 105303 (2016).

³¹M. Higashiwaki, S. Chowdhury, B. L. Swenson, and U. K. Mishra, *Appl. Phys. Lett.* **97**, 222104 (2010).

³²M. Higashiwaki, S. Chowdhury, M.-S. Miao, B. L. Swenson, C. G. Van de Walle, and U. K. Mishra, *J. Appl. Phys.* **108**, 063719 (2010).

³³M. S. Miao, J. R. Weber, and C. G. Van de Walle, *J. Appl. Phys.* **107**, 123713 (2010).

³⁴T. L. Duan, J. S. Pan, and D. S. Ang, *J. Solid State Sci. Technol.* **5**, P514 (2016).

³⁵J. Robertson and B. Falabretti, *J. Appl. Phys.* **100**, 014111 (2006).

³⁶W. Mönch, *J. Appl. Phys.* **80**, 5076 (1996).

³⁷D. Fritsch, H. Schmidt, and M. Grundmann, *Phys. Rev. B* **67**, 235205 (2003).

³⁸J. Robertson, *J. Vac. Sci. Technol. B* **18**, 1785 (2000).